Mathematical Modelling of Engineering Problems
Vol. 11, No. 9, September, 2024, pp. 2388-2404
Journal homepage: http://iieta.org/journals/mmep

Enhanced Displacement Magnification in Symmetrical Differential Levers: A Compliant Mechanism Design Optimization Study

Ngoc Thai Huynh*, Minh Huy Nguyen, Le Cao Ky Dinh, Thanh Dat Vo

Faculty of Mechanical Engineering and Technology, Ho Chi Minh City University of Industry and Trade, Ho Chi Minh City 700000, Vietnam

Corresponding Author Email: thaihn@huit.edu.vn

https://doi.org/10.18280/mmep.110912

Received: 1 April 2024
Revised: 8 July 2024
Accepted: 15 July 2024
Available online: 29 September 2024

Keywords:
grey relational analysis, TOPSIS method, MOORA method, EDAS method, Taguchi method

ABSTRACT

Compliant mechanism work based on the elasticity of material, dimension of the compliant mechanisms and the shape of flexure hinge. In order to larger workspace, most published works use theoretical models to determine the displacement amplification of the mechanical systems, which is very difficult to do. A simpler method that can still achieve efficiency while designing a mechanism with high displacement gain and low stress that ensures a stable working structure is to use combined grey relational analysis Taguchi method is based on the results of finite element analysis in ANSYS. To do this, first select the design variables for the symmetric differential lever displacement amplifier model. Next step, use Minitab software to design 27 cases. Then use SolidWorks to design 27 models of symmetrical differential displacement amplifier. Next to finite element analysis in ANSYS to obtain displacements and stresses of the symmetrical differential lever compliant mechanism with circular flexure hinge. The results obtained from the finite element model are used for optimization by grey relationship analysis combined with the Taguchi method. The FEM results indicated that the designed variables significantly affected on the displacement and stress of the symmetrical differential lever displacement magnification compliant mechanism. The problem was also confirmed by grey relational analysis with Taguchi method. The predicted and optimal values of the displacement were 0.11276 mm and 0.1179 mm, with error of 4.36%. The input displacement was 0.01 mm, while the displacement magnification ratio was 11.79 times. The results verified by decision-making criteria: TOPSIS method, MOORA method and EDAS method.

1. INTRODUCTION

A compliant mechanism using flexure hinge depends on the elasticity of the flexure hinge to function. The workspace of such mechanisms or the displacement amplification ratio requires the large. However, the stress of the mechanical systems has to be low. Thus, this problem poses a major challenge to researchers. Here, in order to create a workspace for a mechanism, a topology optimization was applied to structurally optimize the flexure hinge and mesh beam [1] that were used in a compliant mechanism. The displacement and stress of the bridge type compliant mechanism [2] were determined with the finite element analysis (FEA) model in ANSYS based on the nonlinear and linear. The optimal structure of the flexure joint was selected through topology optimization. A V-shape flexible joint and filleted leaf flexure hinge were then designed for the three-dimensional, bridge-type compliant mechanism. Finite element analysis in ANSYS was used to determine the amplification ratio and relative amplification rate at the millimetre-range, high-frequency compliant mechanism [3]. An experiment was then conducted to confirm the results of the finite element analysis. The hybrid flexure hinges were designed for a bridge-lever-type displacement amplifier for the compliant mechanism to reduce vibration and minimize the disadvantages of the circular hinge with com-like substructures [4]. The high displacement magnification ratio of a bridge-type amplifier compliant mechanism [5] was then obtained based on the fully compliant model. This model was also compared with those of previous studies and was verified with finite element analysis and an experiment. The high displacement magnification of the bridge structure [6] was obtained with changing geometry, stiffness of the material and the topology method. The high displacement amplification ratio of the bridge lever-type amplifier mechanism with the leaf flexure hinge, right circular flexure hinge and V-shape flexure hinge [7] was determined through theoretical finite element analysis and ANSYS. Additionally, an experiment was carried out to confirm the results of the theoretical analysis and simulation. The stiffness and resonant frequency of the oscillation mechanism with flexure hinge [8] was also determined through mathematical modelling. The displacement at the XY micro-motion stage [9] was calculated with mathematically modelled micro-textures, FEA and an experiment. The linear and simplified nonlinear model were run in MATLAB within 140 s. A haft bridge-type amplifier mechanism and parallelogram mechanism were

designed for a microgripper mechanism [10] and manufactured for testing to verify the results of the finite element analysis in ANSYS. Theoretical modelling, force analysis and magnification displacement modelling were used to determine the high displacement amplification of the schematic of the micro/nano-positioning stage with six degrees of freedom [11] and was confirmed with an experiment. The matrix displacement method was combined with the transfer matrix method to analyse the kinetostatics of the mechanical systems [12]. High displacement amplification was obtained through FEA and was verified by experimentation and a previous study. The semi-analytical finite element model, based on Lagrange's equation, was applied to determine displacement and frequency of the mechanism [13]. The result of this method was confirmed with an existing theoretical method and the finite element in ANSYS. The free vibration of a flexure hinge [14] was analysed with a dynamic stiffness matrix model based on a non-uniform Timoshenko beam. The parallel four-bar linkage [15] using a single symmetric flexure hinge and a semi-circular, corner-filleted, and special 6th-order polynomial hinge contour, rigid-body model was designed based on theoretical investigation results and FEA. The model for the experiment was carried out to confirm theoretical and FEA assessments. The 3-revolute-revolute-revolute (RRR) compliant micro motion stage [16] with circular notched flexure hinge was designed using the 3-DOF-pseudo-rigid body model (PRBM). A genetic algorithm was utilized to optimize the workspace of a compact, XY-parallel nanoposition with a small size [17, 18]. An experiment was then carried out to verify the optimal results of the genetic algorithm based on FEA. The high displacement amplification ratio of the bridge-type compliant mechanism [19] was determined using an improved fractional order model and two differential type hysteresis models and was confirmed through an experiment. Then, the high displacement of three popular bridge-type compliant mechanisms [20, 21] was assessed with a two-port dynamic stiffness model and was compared kinetostatics and dynamics of based the design variable changing. An asymmetric compliant mechanism [22] was then created using a novel guiding-bridge-type mechanism, a Scott Russell mechanism and a lever mechanism to improve the dynamic performance of the micro manipulator based on a pseudo-rigid-body model and matrix method. A model for the experiment was also run to confirm the result of the matrix method. Additionally, the pseudo-rigid-body method and the finite element analysis method were applied to determine the high-step efficiency, high speed and precision [23]. The outcomes of these methods were then verified through experimentation. The displacement amplification ratio of the microgripper [24] with a double-stair, bridge-type mechanism was determined through stiffness modelling and was confirmed by FEA and experimentation. The work space of the 6-DOF compliant platform [25] was obtained with a bridge-type amplifier mechanism, a multi-stage condensed modelling method and a kinetostatic model. The obtained results were also compared through FEA and experimentation. A novel mathematical model based on the elastic beam theory and Castigliano's second theorem was also used to determine the displacement amplification ratio of the mechanical structure of the XY stage [26, 27] with a bridge-type amplifier mechanism. The results of this novel method were verified through FEA and experimentation. A type of symmetrical differential lever displacement amplification mechanism [28] was then designed based on the finite element analysis and the results of simulation in ANSYS. The model was manufactured for experimentation to verify the results of the finite element method and the results of ANSYS analysis. The stiffness model developed for electromagnetic mechanism [29] using double parallelogram guiding structures and differential lever amplification structure in compliant mechanism. The simulation results from COMSOL and experiment indicated that the stiffness of the model can change. The DIM and PID control were used to control a 2-DOF compliant positioning stage [30]. The results of this work were confirmed by the experiment and finite element model. The elliptical flexure hinge and hyperbolic hybrid flexure hinge were designed for compliant mechanism [31]. To evaluate the deformation capacity due to proportional stress. Experiments and finite element model used to confirm the deformation capacity and performance of types of flexure hinge. The results pointed out that the hybrid flexure hinge is the most. In order to increase capacity work of flexure hinge a study focused on investigation the change of cross-sectional area of elliptical flexure hinge [32]. The experiment result and finite element model pointed out that this flexure hinge decreased concentration stress. The semi-circular notch flexure hinge [33] for four bar linkage mechanism. The displacement and stress of the proposed model were determined by the finite element analysis and Castigliano's second theorem and experiment.

There is not any research project that has designed 27 the displacement magnification in symmetrical differential lever Compliant Mechanism models using circular flexure hinge and then analyzed the finite element analysis using ANSYS. Strains and stresses obtained from the finite element model are utilized to select optimal case using grey relational analysis combined with the Taguchi method. The results achieved are still compared with the TOPSIS method, the MOORA method and the EDAS method, all of which choose the first case as the optimal case. Previous studies have used the theoretical analysis method, FEA and experimentation to obtain the desired displacement amplification ratio. However, these methods did not achieve a high amplification ratio, which is difficult to accomplish. Thus, this investigation presented an improved approach in the following ways:

- Grey relational analysis was applied to determine the optimal amplification ratio of a novel symmetrical differential lever displacement magnification compliant mechanism based on FEA in ANSYS.
- The optimal results of grey relational analysis were also confirmed with the TOPSIS method, the MOORA method, the EDAS method and the Taguchi method.
- Four optimization methods were implemented, all of which used the MEREC weight measurement technique.
- Five optimization methods also confirmed that the first case was the optimal case.

The rest of this study is presented as follows: the design of a novel symmetrical differential lever displacement magnification compliant mechanism and finite element model are presented in Section 2; optimal methods are analysed in Section 3; the results are analysed and discussed in Section 4; conclusions are described in Section 5; references are provided for all cited work.

2. DESIGN MODELLING AND FINITE ELEMENT ANALYSIS

2.1 Design modelling of a novel symmetrical differential lever displacement magnification compliant mechanism

The study model designed in this investigation is an improved symmetrical differential lever displacement magnification compliant mechanism using five optimization methods based on finite element analysis in ANSSYS. Twenty-seven mechanism models were designed using SolidWorks, as depicted in Figure 1. The overall dimension of the study model was presented in Figure 2. The design variables included the following: the distance dimension was variable A, the thickness of flexure hinge was variable B, all radius of the flexure hinge was variable C, and the radius of the two flexures below the model, as shown in Figure 2, was variable D.

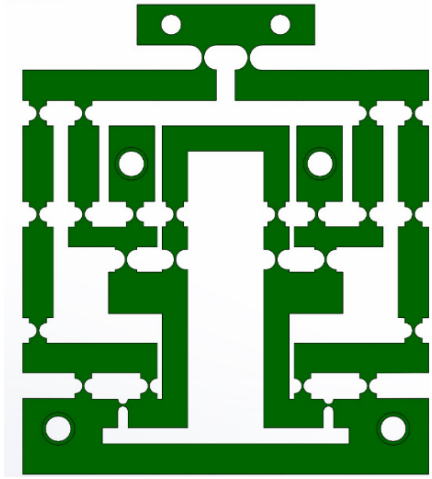

Figure 1. A novel symmetrical differential lever displacement magnification compliant mechanism

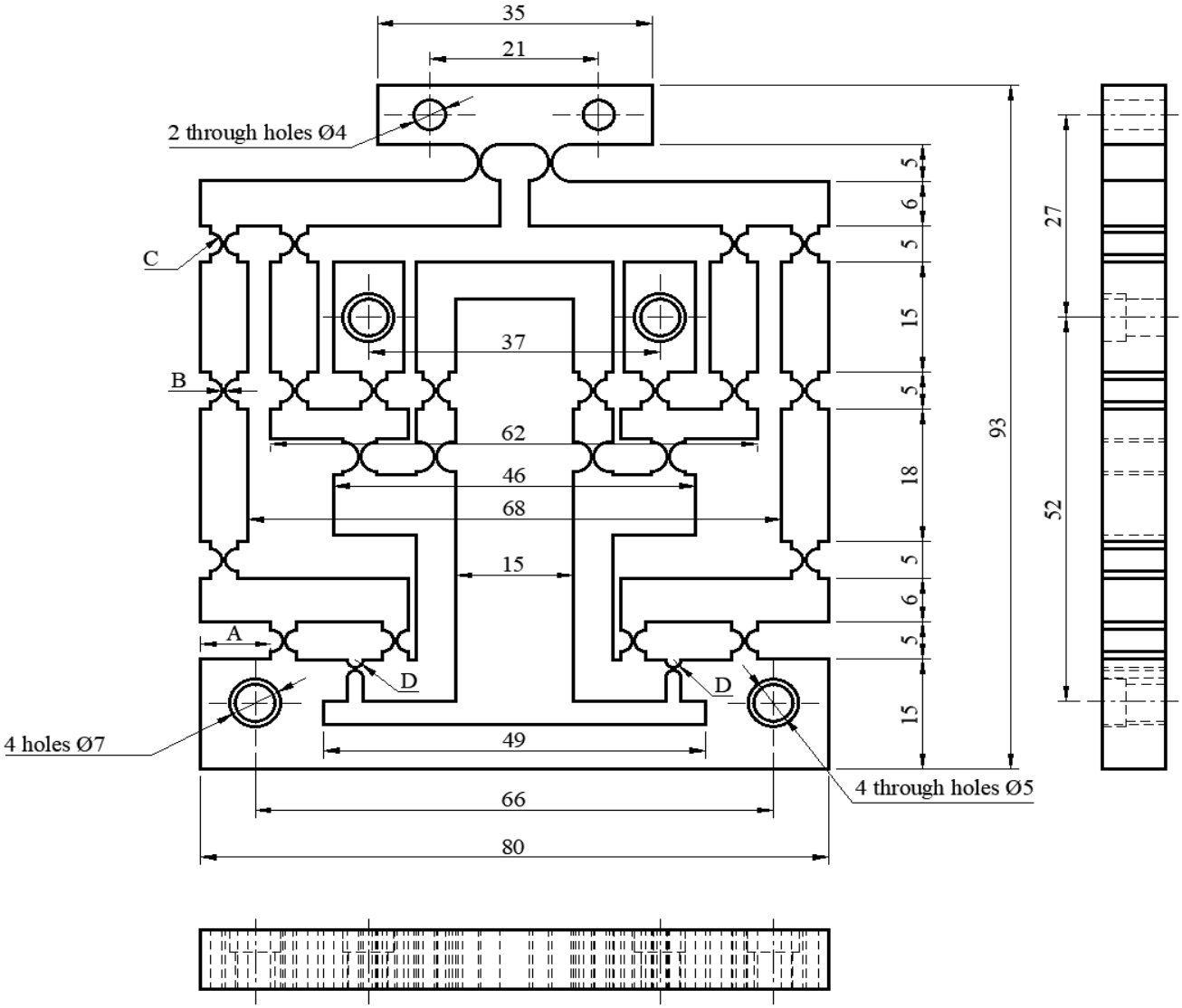

Figure 2. The projection of a novel symmetrical differential lever displacement magnification compliant mechanism

2.2 Finite element analysis

The finite element model was set up in ANSYS as follows:

The Al 6061-T6 material was selected for the mechanism in this investigation. The mesh was divided using the automatic method with meshing size of 0.5, 57826 nodes and 35865 elements, as illustrated in Figure 3(a). The model was set up for simulation as shown in Figure 3(b). Four holes were selected as the fixed support. Surfaces B and C were selected for input of displacement of 0.01 mm.

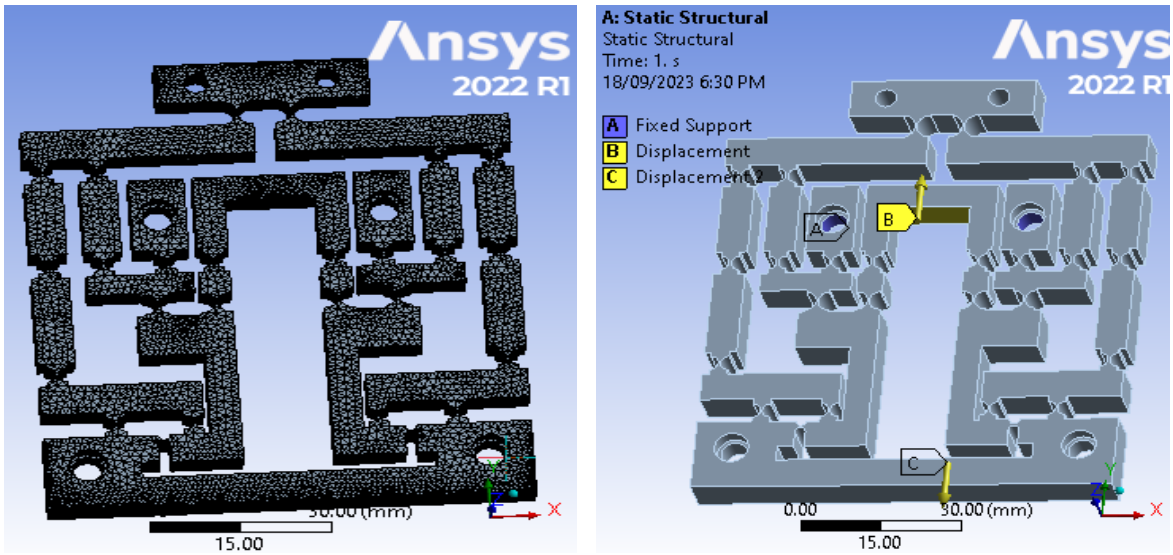

(a) Divided mesh (b) Input boundary condition

Figure 3. Divided mesh and input boundary condition for the model

3. OPTIMIZATION METHOD

3.1 Estimating weight using the MEREC method

The weights of optimal objectives were determined with MEREC method [34-40] as follows:

Step 1: The criteria of the objective were determined.

$$h_{ij} = \frac{\min u_{ij}}{u_{ij}} \tag{1}$$

$$h_{ij} = \frac{u_{ij}}{\max u_{ij}} \tag{2}$$

where, u_{ij} is the output value. In this investigation, u_{ij} represents the values of displacement and stress, which were obtained from finite element analysis with ANSYS.

Step 2: Total performance of the criteria was determined.

$$S_i = \ln\left[1+\left(\frac{1}{n}\sum_{j}^{n}\left|\ln(h_{ij})\right|\right)\right] \tag{3}$$

Step 3: The performance of the criteria was determined.

$$S_{ij}^{'} = \ln\left[1+\left(\frac{1}{n}\sum_{k,k\neq j}^{n}\left|\ln(h_{ij})\right|\right)\right] \tag{4}$$

Step 4: The deviation was determined.

$$E_j = \left|S_{ij}^{'} - S_i\right| \tag{5}$$

Step 5: The weight of every criterion was determined.

$$w_j = \frac{E_j}{\sum_k^m E_k} \tag{6}$$

3.2 Grey relational analysis

Grey theory was widely applied to the system where the model was uncertain or the information was incomplete. This supplied an effective solution to the problem of uncertainty through multiple discrete inputs. Grey relational analysis (GRA), which is a part of grey systems theory, is suitable for solving multiple factors [41-48] as follows:

Step 1: The values of objective function were determined.

$$D_i^* = \frac{D_i^{(0)}(k) - \min D_i^0(k)}{\max D_i^{(0)}(k) - \min D_i^{(0)}(k)} \tag{7}$$

$$D_i^* = \frac{\max D_i^{(0)}(k) - D_i^0(k)}{\max D_i^{(0)}(k) - \min D_i^{(0)}(k)} \tag{8}$$

where, $D_i^{(0)}(k)$ is the output value. In this investigation, $D_i^{(0)}(k)$ represents the values of displacement and stress, which were obtained from finite element analysis with ANSYS.

Step 2: Calculation deviation.

$$\Delta_{0i} = \left\|D_0^*(k) - D_i^*(k)\right\| \tag{9}$$

$$\Delta_{\min} = \max_{\forall j\in i}\min_{\forall k}\left\|D_0^*(k) - D_j^*(k)\right\| \tag{10}$$

$$\Delta_{\max} = \max_{\forall j\in i}\max_{\forall k}\left\|D_0^*(k) - D_j^*(k)\right\| \tag{11}$$

Step 3: The grey relational coefficient (GRC) (γ) was estimated as follows:

$$\gamma_i(k) = \frac{\Delta_{\min} + \xi\Delta_{\max}}{\Delta_{0i} + \xi.\Delta_{\max}} \tag{12}$$

Here, $\xi \in [0,1]$ is the distinguishing coefficient, usually 0.5.

Step 4: GRG (ψ_i) was computed as follows:

$$\psi_i = \sum_{k=1}^{n} w_k \gamma_i(k) \tag{13}$$

where, n is the quantity of the experiment and w_k is the weight of every criterion that was determined with the MEREC method.

Step 5: The rank of the GRG value was determined to confirm the optimal values according to the principle that the maximum value of the GRG is the optimal value.

3.3 TOPSIS method

The TOPSIS method is a multi-criteria decision-making method. With the desire that the proposed model has high amplification and low stress. This is a multi-objective optimization problem. Therefore, the application of EDAs method is necessary to confirm the optimal case of the design variables of the grey-Taguchi method. The TOPSIS method [49-54] was used to confirm the optimal values of displacement and stress of the novel bridge -type amplifier as follows:

Step 1: The normalized values of the criteria were determined.

$$n_{ij} = \frac{u_{ij}}{\sqrt{\sum_{i=1}^{n} u_{ij}^2}} \tag{14}$$

where, u_{ij} is the output values. In this investigation, u_{ij} represents the values of displacement and stress, which were obtained from finite element analysis with ANSYS.

Step 2: The weighted normalized values of the criteria were determined.

$$v_{ij} = \mathrm{w}_i n_{ij} \tag{15}$$

where, W_i is the weight of every criterion and was determined by MEREC.

Step 3: The maximum values and the minimum values were determined according to the criteria of the objective functions.

$$v^+ = (v_1^+, v_2^+, \ldots v_n^+) \tag{16}$$

$$v^- = (v_1^-, v_2^-, \ldots v_n^-) \tag{17}$$

Step 4: The values of S_i^+ and S_i^- of the optimal criteria were determined.

$$S_i^+ = \sqrt{\sum_{j=1}^{n} (v_{ij} - v_j^+)^2} \tag{18}$$

$$S_i^- = \sqrt{\sum_{j=1}^{n} (v_{ij} - v_j^-)^2} \tag{19}$$

Step 5: The value of B_i was determined.

$$B_i = \frac{S_i^-}{S_i^+ + S_i^-} \tag{20}$$

Step 6: The rank of the B_i value was determined to confirm the optimal values according to the principle that the maximum value of B_i is the optimal value.

3.4 MOORA method

The MOORA method is a multi-criteria decision-making method. With the desire that the proposed model has high amplification and low stress. This is a multi-objective optimization problem. Therefore, the application of EDAs method is necessary to confirm the optimal case of the design variables of the grey-Taguchi method. The MOORA method [55-57] was used to confirm the optimal results of grey relational analysis and TOPSIS method and was carried out as follows:

Step 1: The normalized values of the criteria were determined:

$$n_{ij} = \frac{u_{ij}}{\sqrt{\sum_{i=1}^{n} u_{ij}^2}} \tag{21}$$

where, u_{ij} represents the output values. In this investigation, u_{ij} represents the values of displacement and stress which were obtained from finite element analysis with ANSYS.

Step 2: The weighted normalized values of the criteria were determined.

$$v_{ij} = \mathrm{w}_i n_{ij} \tag{22}$$

where, W_i is the weight of every criterion and was determined by MEREC.

Step 3: Q_i was calculated as following as:

$$Q_i = \sum_{j=1}^{g} v_{ij} - \sum_{j=g+1}^{n} v_{ij} \tag{23}$$

Step 4: The alternatives were ranked according to the principle that the option with the highest value of Q_i is the best.

3.5 EDAS method

The EDAS method is a multi-criteria decision-making method. With the desire that the proposed model has high amplification and low stress. This is a multi-objective optimization problem. Therefore, the application of EDAs method is necessary to confirm the optimal case of the design variables of the grey-Taguchi method. The steps for implementing the EDAS method [58-60] for multi-criteria decisions were as follows:

Step 1: The decision matrix was built according to the formula:

$$X = [x_{ij}]_{m \times n} = \begin{bmatrix} x_{11} & \cdots & x_{1n} \\ x_{21} & \cdots & x_{1n} \\ \vdots & \cdots & x_{2n} \\ x_{m1} & \cdots & x_{mn} \end{bmatrix} \tag{24}$$

The number of options is m, the number of criteria is n, and x_{ij} is the value of criterion j at option i.

Step 2: The average value (AVG) of the alternatives was

determined:

$$AVG = \frac{\sum_{i=1}^{m} x_i}{m} \quad (25)$$

Step 3: The positive distance (PD) and negative distance (ND) were determined from the average:

$$PD_{ij} = \frac{\max[0,(x_{ij} - AVG_j)]}{AVG_j} \quad (26)$$

$$PD_{ij} = \frac{\max[0,(AVG_j - x_{ij})]}{AVG_j} \quad (27)$$

$$ND_{ij} = \frac{\max[0,(AVG_j - x_{ij})]}{AVG_j} \quad (28)$$

$$ND_{ij} = \frac{\max[0,(x_{ij} - AVG_j)]}{AVG_j} \quad (29)$$

Step 4: The total positive distance (SoP) and total negative distance (SoN) were calculated.

$$SoP_i = \sum_{i=1}^{m} w_j . PD_{ij} \quad (30)$$

$$SoN_i = \sum_{i=1}^{m} w_j . ND_{ij} \quad (31)$$

W_j is the weight of criterion j.

Step 5: SoP and SoN values were normalized according to the formula:

$$SSoP_i = \frac{SoP_i}{\max(SoP_i)} \quad (32)$$

$$SSoN_i = \frac{SoN_i}{\max(SoN_i)} \quad (33)$$

Step 6: The evaluation score (APS_i) of the options was calculated according to the formula:

$$APS_i = \frac{1}{2}(SSoP_i + SSoN_i) \quad (34)$$

Step 7: Alternatives were ranked according to the rule that the option with the highest score is the best.

3.6 Taguchi method

In this method, the signal to noise for GRG, B_i, Q_i and APS_i was analysed with the objective function 'the maximum is the better' [61-66] as follows:

$$S/N = -10\log(\frac{1}{n}\sum_{i=1}^{n}\frac{1}{y_i^2}) \quad (35)$$

y_i is value of the i[th] simulation and n is the total number of simulation.

3.7 Determining the predicted values: GRG, B_i, Q_i and APS_i

The predicted value of GRG was obtained as follows:

$$\mu_G = G_m + \sum_{i=1}^{q}(G_0 - G_m) \quad (36)$$

CI value was also determined at $\alpha=0.05$ for GRG B_i, Q_i and APS_i by employing Eq. (37):

$$CI_{CE} = \pm\sqrt{F_\alpha(1, fe)Ve(\frac{1}{n_{eff}} + \frac{1}{R_e})} \quad (37)$$

$F_\alpha(1, fe)$ value look up in Table B-2 in reference [67].

4. RESULTS AND DISCUSSION

The design variables for this study, as pointed out in Figure 2, consisted of the distance dimension (variable A) with three levels of 9 mm, 11 mm and 13 mm, thickness of the flexure hinge (variable B) with three levels of 0.3 mm, 0.4 mm and 0.5 mm, radius of the flexure hinge 1 (variable C) with three levels of 1.5 mm, 2 mm and 2.5 mm, and radius of the flexure hinge 2 (variable D) with three levels of 1 mm, 1.25 mm and 1.5 mm as presented in Table 1.

Table 1. The design variables and their level

Design Variables	Symbol	Unit	Level 1	Level 2	Level 3
Distance dimension	A	mm	9	11	13
Thickness of circular flexure hinge	B	mm	0.3	0.4	0.5
Radius of flexure hinge 1	C	mm	1.5	2	2.5
Radius of flexure hinge 2	D	mm	1	1.25	1.5

4.1 Simulation set-up

The orthogonal array L_{27} was created with Minitab software. We sought to create 27 models in order to determine output displacement and output stress through finite element analysis in ANSYS. The boundary condition was set up as follows: four holes were fixed with a fixed support tool. The initial condition was an input displacement of 0.01 and was set up for surface B and C. The orthogonal array and the results of the displacement and stress of finite element analysis are listed in Table 2. In this Table indicated that the design variables significantly affected the displacement and stress. Because the results of the displacement and stress of the 27 different models were not the same. When the design variables: distance dimension (A), thickness of circular flexure hinge**,** the radius of circular flexure hinges changed the displacement and stress were also changed. The problem indicated that the design variables significantly changed on the displacement and stress. Therefore, while designing this model, these design variables must not be ignored.

4.2 Determining weight

Displacement and stress values were used to determine the weight for every output. By substituting all displacement and stress values in Eqs. (1)-(6), the results were obtained as shown in Table 3. Finally, the weights of output displacement and stress were found to be 0.4815 and 0.5185, respectively.

Table 2. Orthogonal array and the FEM

Trial No.	A (mm)	B (mm)	C (mm)	D (mm)	Displacement (Di) (mm)	Stress (St) (MPa)
1	9	0.3	1.5	1	0.1179	84.113
2	9	0.3	2	1.25	0.1242	101.51
3	9	0.3	2.5	1.5	0.1096	105.80
4	9	0.4	1.5	1.25	0.0862	83.87
5	9	0.4	2	1.5	0.1191	124.58
6	9	0.4	2.5	1	0.1141	116.28
7	9	0.5	1.5	1.5	0.0803	69.59
8	9	0.5	2	1	0.1076	103.17
9	9	0.5	2.5	1.25	0.1093	118.13
10	11	0.3	1.5	1	0.0863	81.64
11	11	0.3	2	1.25	0.1113	130.58
12	11	0.3	2.5	1.5	0.0956	120.62
13	11	0.4	1.5	1.25	0.0791	85.68
14	11	0.4	2	1.5	0.1109	121.74
15	11	0.4	2.5	1	0.1029	119.40
16	11	0.5	1.5	1.5	0.0749	86.92
17	11	0.5	2	1	0.0742	102.94
18	11	0.5	2.5	1.25	0.0986	126.75
19	13	0.3	1.5	1	0.0892	70.27
20	13	0.3	2	1.25	0.1034	117.89
21	13	0.3	2.5	1.5	0.0856	122.26
22	13	0.4	1.5	1.25	0.0721	82.59
23	13	0.4	2	1.5	0.1022	139.32
24	13	0.4	2.5	1	0.0922	123.07
25	13	0.5	1.5	1.5	0.0692	88.24
26	13	0.5	2	1	0.0687	100.54
27	13	0.5	2.5	1.25	0.0902	127.09

Table 3. Results of the MEREC method

	h_{ij}		S_i		$S_{ij'}$		E_j
	Di	St		Di	St	Di	St
1	0.5827	0.6077	0.4181	0.2391	0.2223	0.1790	0.0167
2	0.5531	0.7286	0.3746	0.2593	0.1470	0.1152	0.1124
3	0.6268	0.7594	0.3157	0.2099	0.1289	0.1058	0.0810
4	0.7970	0.6020	0.3128	0.1075	0.2261	0.2053	0.1187
5	0.5768	0.8942	0.2859	0.2430	0.0544	0.0429	0.1886
6	0.6021	0.8346	0.2957	0.2261	0.0865	0.0696	0.1395
7	0.8555	0.4995	0.3542	0.0751	0.2979	0.2791	0.2228
8	0.6385	0.7405	0.3181	0.2024	0.1399	0.1157	0.0625
9	0.6285	0.8479	0.2736	0.2088	0.0793	0.0648	0.1295
10	0.7961	0.5860	0.3230	0.1080	0.2368	0.2150	0.1288
11	0.6173	0.9373	0.2419	0.2161	0.0319	0.0258	0.1842
12	0.7186	0.8658	0.2129	0.1529	0.0696	0.0600	0.0833
13	0.8685	0.6150	0.2727	0.0681	0.2176	0.2046	0.1495
14	0.6195	0.8738	0.2676	0.2147	0.0653	0.0530	0.1494
15	0.6676	0.8570	0.2462	0.1840	0.0743	0.0622	0.1097
16	0.9172	0.6239	0.2462	0.0423	0.2118	0.2039	0.1695
17	0.9259	0.7389	0.1738	0.0378	0.1409	0.1360	0.1031
18	0.6968	0.9098	0.2053	0.1661	0.0462	0.0393	0.1199
19	0.7702	0.5044	0.3872	0.1227	0.2943	0.2644	0.1716
20	0.6644	0.8462	0.2530	0.1860	0.0802	0.0670	0.1058
21	0.8026	0.8775	0.1615	0.1043	0.0633	0.0572	0.0411
22	0.9528	0.5928	0.2512	0.0239	0.2323	0.2274	0.2084
23	0.6722	1.0000	0.1811	0.1811	0.0000	0.0000	0.1811
24	0.7451	0.8834	0.1899	0.1372	0.0602	0.0526	0.0771
25	0.9928	0.6334	0.2086	0.0036	0.2057	0.2050	0.2021
26	1.0000	0.7216	0.1511	0.0000	0.1511	0.1511	0.1511
27	0.7616	0.9122	0.1673	0.1276	0.0449	0.0396	0.0827

4.3 The results of the grey relational analysis

The results of the objective function were obtained by substituting the displacement and stress values in Table 2 into Eq. (7) and Eq. (8). The deviation values of the objective function were then determined by substituting the values of the

objective function into Eq. (9). Then, Eq. (10) and Eq. (11) were used to calculate the minimum and maximum values of the deviation value. The grey relational coefficient was determined using Eq. (12), while Eq. (13) was used to determine the grey relational grade values. The maximum value of the grey relational grade was ranked first. This maximum value indicated that the first case was the optimal case. The optimal value of the grey relational grade obtained was 0.7612. The twenty-seven values of the grey relational grade were not the same. Thus, this problem proves that the designed variables significantly affected the output displacement and stress. All the results of grey relational analysis method strongly agreed agree with the finite element analysis, as listed in Table 4.

Table 4. The values of objective functions, deviation, grey relational coefficient, grey relational grade and rank

Orde Experiment	D_i^* (1)	D_i^* (2)	Δ_{0i} (1)	Δ_{0i} (2)	γ_i (1)	γ_i (2)	(ψ_i)	Rank
1	0.8860	0.7840	0.1140	0.2160	0.8143	0.6983	0.7612	1
2	1.0000	0.5420	0.0000	0.4580	1.0000	0.5219	0.7521	2
3	0.7370	0.4810	0.2630	0.5190	0.6553	0.4907	0.5700	9
4	0.3150	0.7950	0.6850	0.2050	0.4219	0.7092	0.5709	8
5	0.9080	0.2110	0.0920	0.7890	0.8446	0.3879	0.6078	5
6	0.8180	0.3300	0.1820	0.6700	0.7331	0.4274	0.5746	7
7	0.2090	1.0000	0.7910	0.0000	0.3873	1.0000	0.7050	4
8	0.7010	0.5180	0.2990	0.4820	0.6258	0.5092	0.5653	10
9	0.7320	0.3040	0.2680	0.6960	0.6510	0.4181	0.5303	14
10	0.3170	0.8270	0.6830	0.1730	0.4227	0.7429	0.5887	6
11	0.7680	0.1250	0.2320	0.8750	0.6831	0.3636	0.5175	16
12	0.4850	0.2680	0.5150	0.7320	0.4926	0.4058	0.4476	20
13	0.1870	0.7690	0.8130	0.2310	0.3808	0.6840	0.5380	12
14	0.7600	0.2520	0.2400	0.7480	0.6757	0.4006	0.5331	13
15	0.6160	0.2860	0.3840	0.7140	0.5656	0.4119	0.4859	19
16	0.1120	0.7510	0.8880	0.2490	0.3602	0.6676	0.5196	15
17	0.0990	0.5220	0.9010	0.4780	0.3569	0.5112	0.4369	23
18	0.5390	0.1800	0.4610	0.8200	0.5203	0.3788	0.4469	21
19	0.3690	0.9900	0.6310	0.0100	0.4421	0.9804	0.7212	3
20	0.6250	0.3070	0.3750	0.6930	0.5714	0.4191	0.4924	18
21	0.3050	0.2450	0.6950	0.7550	0.4184	0.3984	0.4080	27
22	0.0610	0.8140	0.9390	0.1860	0.3475	0.7289	0.5452	11
23	0.6040	0.0000	0.3960	1.0000	0.5580	0.3333	0.4415	22
24	0.4230	0.2330	0.5770	0.7670	0.4643	0.3946	0.4282	25
25	0.0090	0.7330	0.9910	0.2670	0.3353	0.6519	0.4994	17
26	0.0000	0.5560	1.0000	0.4440	0.3333	0.5297	0.4351	24
27	0.3870	0.1750	0.6130	0.8250	0.4492	0.3774	0.4120	26

Table 5. The normalized values, the weighted normalized values of the criteria, S_i^+, S_i^-, and rank

Order Experiment	n_{ij}		v_{ij}		S_i^+	S_i^-	B_i	Rank
	Di	St	Di	St				
1	0.2346	0.1515	0.1129	0.0786	0.0152	0.0692	0.8196	1
2	0.2471	0.1816	0.1190	0.0942	0.0296	0.0637	0.6826	2
3	0.2180	0.1893	0.1050	0.0982	0.0364	0.0500	0.5789	8
4	0.1715	0.1501	0.0826	0.0778	0.0387	0.0541	0.5828	7
5	0.2369	0.2229	0.1141	0.1156	0.0513	0.0502	0.4947	13
6	0.2270	0.2081	0.1093	0.1079	0.0444	0.0485	0.5220	10
7	0.1598	0.1245	0.0769	0.0646	0.0421	0.0656	0.6095	4
8	0.2141	0.1846	0.1031	0.0957	0.0350	0.0501	0.5890	6
9	0.2174	0.2114	0.1047	0.1096	0.0472	0.0436	0.4799	14
10	0.1717	0.1461	0.0827	0.0757	0.0380	0.0561	0.5963	5
11	0.2214	0.2337	0.1066	0.1211	0.0579	0.0416	0.4181	19
12	0.1902	0.2158	0.0916	0.1119	0.0547	0.0311	0.3622	22
13	0.1574	0.1533	0.0758	0.0795	0.0457	0.0508	0.5261	9
14	0.2206	0.2178	0.1062	0.1129	0.0500	0.0436	0.4656	15
15	0.2047	0.2137	0.0986	0.1108	0.0505	0.0376	0.4268	18
16	0.1490	0.1555	0.0718	0.0806	0.0499	0.0490	0.4954	12
17	0.1476	0.1842	0.0711	0.0955	0.0570	0.0342	0.3746	20
18	0.1962	0.2268	0.0945	0.1176	0.0584	0.0309	0.3461	23
19	0.1775	0.1257	0.0855	0.0652	0.0335	0.0670	0.6664	3
20	0.2057	0.2110	0.0991	0.1094	0.0490	0.0387	0.4413	17
21	0.1703	0.2188	0.0820	0.1134	0.0613	0.0226	0.2698	27
22	0.1434	0.1478	0.0691	0.0766	0.0513	0.0527	0.5066	11
23	0.2033	0.2493	0.0979	0.1293	0.0680	0.0321	0.3205	24
24	0.1834	0.2202	0.0883	0.1142	0.0583	0.0271	0.3172	25
25	0.1377	0.1579	0.0663	0.0819	0.0555	0.0474	0.4608	16
26	0.1367	0.1799	0.0658	0.0933	0.0604	0.0360	0.3732	21
27	0.1794	0.2274	0.0864	0.1179	0.0625	0.0235	0.2734	26

Table 6. The normalized values, the weighted normalized values of the criteria, Q_i and rank

Order Experiment	n_{ij}		v_{ij}		Q_i	Rank
	Di	St	Di	St		
1	0.2346	0.1515	0.11295	0.07855	0.03440	1
2	0.2471	0.1816	0.11898	0.09418	0.02481	2
3	0.2180	0.1893	0.10500	0.09816	0.00684	7
4	0.1715	0.1501	0.08258	0.07781	0.00477	8
5	0.2369	0.2229	0.11410	0.11558	-0.00148	10
6	0.2270	0.2081	0.10931	0.10788	0.00143	9
7	0.1598	0.1245	0.07693	0.06456	0.01237	4
8	0.2141	0.1846	0.10308	0.09572	0.00737	5
9	0.2174	0.2114	0.10471	0.10959	-0.00488	12
10	0.1717	0.1461	0.08268	0.07574	0.00693	6
11	0.2214	0.2337	0.10663	0.12114	-0.01452	18
12	0.1902	0.2158	0.09159	0.11190	-0.02032	20
13	0.1574	0.1533	0.07578	0.07949	-0.00371	11
14	0.2206	0.2178	0.10624	0.11294	-0.00670	13
15	0.2047	0.2137	0.09858	0.11077	-0.01219	17
16	0.1490	0.1555	0.07175	0.08064	-0.00889	15
17	0.1476	0.1842	0.07108	0.09550	-0.02442	22
18	0.1962	0.2268	0.09446	0.11759	-0.02313	21
19	0.1775	0.1257	0.08545	0.06519	0.02026	3
20	0.2057	0.2110	0.09906	0.10937	-0.01031	16
21	0.1703	0.2188	0.08201	0.11343	-0.03142	26
22	0.1434	0.1478	0.06907	0.07662	-0.00755	14
23	0.2033	0.2493	0.09791	0.12925	-0.03135	25
24	0.1834	0.2202	0.08833	0.11418	-0.02585	23
25	0.1377	0.1579	0.06629	0.08186	-0.01557	19
26	0.1367	0.1799	0.06581	0.09328	-0.02746	24
27	0.1794	0.2274	0.08641	0.11791	-0.03150	27

Table 7. Positive distance, negative distance, SoP_i, SoN_i, $SSoP_i$, $SSoN_i$, APS_i, and rank

Order	*PDij*		*NDij*							
Experiment	Di	St	Di	St	SoP_i	SoN_i	$SSoP_i$	$SSoN_i$	APS_i	Rank
1	0.23628	0.19930	0.00000	0.00000	0.21711	0.00000	1.00000	1.00000	1.00000	1
2	0.30234	0.04006	0.00000	0.00000	0.16636	0.00000	0.76626	1.00000	0.88313	2
3	0.14925	0.00000	0.00000	0.00051	0.07187	0.00026	0.33104	0.99839	0.66471	6
4	0.00000	0.20687	0.09612	0.00000	0.10725	0.04629	0.49401	0.71881	0.60641	8
5	0.24886	0.00000	0.00000	0.17811	0.11984	0.09234	0.55199	0.43903	0.49551	10
6	0.19643	0.00000	0.00000	0.09962	0.09459	0.05165	0.43570	0.68624	0.56097	9
7	0.00000	0.34191	0.15799	0.00000	0.17727	0.07608	0.81649	0.53782	0.67715	4
8	0.12828	0.02436	0.00000	0.00000	0.07440	0.00000	0.34269	1.00000	0.67135	5
9	0.14610	0.00000	0.00000	0.11711	0.07036	0.06072	0.32406	0.63114	0.47760	11
10	0.00000	0.22796	0.09507	0.00000	0.11819	0.04578	0.54437	0.72187	0.63312	7
11	0.16707	0.00000	0.00000	0.23485	0.08045	0.12176	0.37057	0.26032	0.31545	18
12	0.00245	0.00000	0.00000	0.14066	0.00118	0.07292	0.00543	0.55698	0.28120	20
13	0.00000	0.18976	0.17057	0.00000	0.09838	0.08214	0.45314	0.50101	0.47707	12
14	0.16288	0.00000	0.00000	0.15125	0.07843	0.07842	0.36127	0.52362	0.44245	13
15	0.07899	0.00000	0.00000	0.12912	0.03804	0.06694	0.17521	0.59332	0.38426	17
16	0.00000	0.17803	0.21461	0.00000	0.09230	0.10335	0.42514	0.37217	0.39865	16
17	0.00000	0.02653	0.22195	0.00000	0.01376	0.10688	0.06337	0.35070	0.20703	22
18	0.03390	0.00000	0.00000	0.19863	0.01633	0.10298	0.07520	0.37440	0.22480	21
19	0.00000	0.33548	0.06466	0.00000	0.17393	0.03114	0.80113	0.81083	0.80598	3
20	0.08424	0.00000	0.00000	0.11484	0.04056	0.05954	0.18684	0.63829	0.41256	14
21	0.00000	0.00000	0.10241	0.15617	0.00000	0.13028	0.00000	0.20853	0.10427	25
22	0.00000	0.21898	0.24397	0.00000	0.11353	0.11748	0.52292	0.28628	0.40460	15
23	0.07165	0.00000	0.00000	0.31750	0.03450	0.16461	0.15893	0.00000	0.07946	27
24	0.00000	0.00000	0.03321	0.16383	0.00000	0.10093	0.00000	0.38687	0.19343	23
25	0.00000	0.16555	0.27438	0.00000	0.08583	0.13213	0.39533	0.19732	0.29632	19
26	0.00000	0.04923	0.27962	0.00000	0.02552	0.13465	0.11756	0.18198	0.14977	24
27	0.00000	0.00000	0.05418	0.20184	0.00000	0.13073	0.00000	0.20578	0.10289	26

4.4 Results of the TOPSIS method

The normalized values of the criteria were determined by substituting the displacement and stress values in Table 2 into Eq. (14). All results of the TOPSIS method are shown in Table 5. The maximum and minimum values of the objective functions were calculated by multiplying the normalized values of the criteria by the weight of output displacement and stress according to Eq. (15). The values of S_i^+ and S_i^- were found with Eqs. (18)-(19). Then, the B_i values were determined using Eq. (20). The maximum value of B_i was ranked first, with this maximum value pointing out that the

first case was the optimal case. The optimal value of B_i obtained was 0.8196. Twenty-seven values of B_i were not the same. This problem thus indicates that the designed variables significantly affected output displacement and stress. This result is exactly the same as that found by grey relational analysis and finite element analysis.

4.5 Results of the MOORA method

The results of MOORA method are presented in Table 6. Normalized values were determined by substituting the displacement and stress values in Table 2 into Eq. (21). The weighted normalized values of the criteria were determined by substituting normalized values of the displacement and stress values into Eq. (22). Q_i values were calculated using Eq. (23). The maximum value of Q_i was ranked first, with this maximum value indicating that the first case was the optimal case. The optimal value of Q_i obtained was 0.03440. Twenty-seven values of Q_i are not the same. Thus, this shows that the designed variables significantly affected output displacement and stress. This result agrees completely with those of the grey relational analysis, TOPSIS method and finite element analysis.

4.6 Results of the EDAS method

The results of EDAS method are presented in Table 7. The positive distance (PD) values were obtained by substituting the displacement and stress values in Table 2 into Eqs. (26)-(27). The negative distance (PD) values were obtained by substituting the displacement and stress values in Table 2 into Eqs. (28)-(29). SoP_i values were obtained by substituting the positive distance of displacement and stress value into Eq. (30). The SoN_i values were obtained by substituting the negative distance of displacement and stress value into Eq. (31). $SSoP_i$ values were obtained by substituting the SoP_i values into Eq. (32). $SSoN_i$ values were obtained by substituting SoN_i values into Eq. (33). APS_i values were obtained by substituting the SoP_i values and the $SSoN_i$ values into Eq. (34). The maximum value of APS_i was ranked first, indicating that the first case was the optimal case. The optimal value of APS_i was found to be 1.000. Twenty-seven values of APS_i are not the same. This problem demonstrates that the designed variables significantly affected output displacement and stress. This result is in complete agreement with the results of the grey relational analysis, the TOPSIS method, the MOORA method, and finite element analysis.

Table 8. Response table for signal-to-noise ratios

Level	A	B	C	D
1	-4.146	-4.877	-4.463	-5.302
2	-6.033	-5.651	-5.624	-5.564
3	-6.386	-6.037	-6.479	-5.700
Delta	2.240	1.160	2.016	0.398
Rank	1	3	2	4

4.7 Results of signal to noise analysis

Results of analysis of signal to noise for GRG are shown in Table 8. In Table 8, the average values of variables A, B, C and D are shown by level in columns 2, 3n, 4 and 5, respectively. The values of delta demonstrate that the variables significantly affected output displacement and stress, next to is variable C, variable B and final is variable D. The data of Table 8 were also used to plot the graph as shown in Figure 4. This figure shows that variable A significantly affected output displacement and stress. Next to it is variable C, variable B and final is variable D. As the slope of the graph increases, the influence increases.

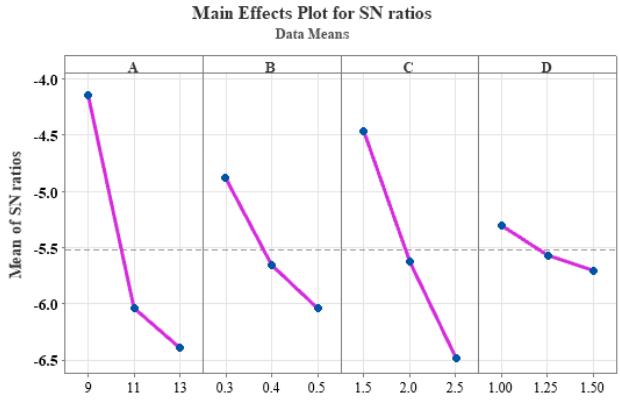

Figure 4. The graph analysis of signal to noise for GRG

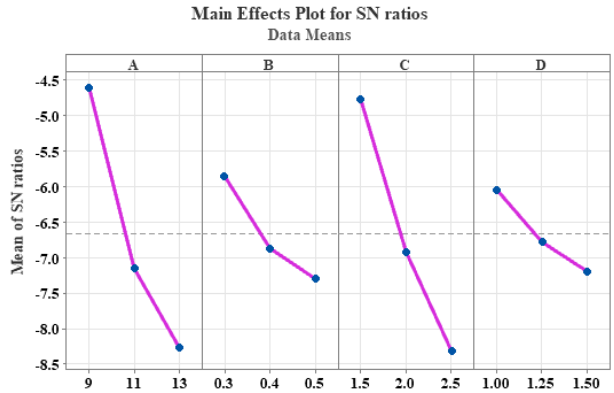

Figure 5. The graph analysis of signal-to-noise ratios for B_i

Table 9. Response table for signal to noise ratios B_i

Level	A	B	C	D
1	-4.613	-5.854	-4.783	-6.050
2	-7.149	-6.869	-6.924	-6.781
3	-8.259	-7.297	-8.314	-7.191
Delta	3.646	1.443	3.530	1.141
Rank	1	3	2	4

Table 10. Response table for signal-to-noise ratios for APS_i

Level	A	B	C	D
1	-3.706	-6.538	-5.157	-7.453
2	-9.051	-9.045	-9.733	-8.507
3	-13.348	-10.523	-11.215	-10.147
Delta	9.642	3.985	6.058	2.694
Rank	1	3	2	4

The results of analysis of the signal-to-noise ratio for B_i are presented in Table 9. In this Table, the average values of variables A, B, C and D are illustrated by level in columns 2, 3n, 4 and 5, respectively. The values of delta show that the variables significantly affected output displacement and stress, next to is variable C, variable B and final is variable D. The data of Table 9 were also used to plot the graph as shown in

Figure 5, which shows that variable A significantly affected on output displacement and stress. next to is variable C, variable B and final is variable D. As the slope of the graph increases, the influence increases.

The results of analysis of the signal-to-noise ratios for APS_i are presented in Table 10. In this table, the average values of variables A, B, C and D are illustrated by level in columns 2, 3n, 4 and 5, respectively. The values of delta indicate that the variables significantly affected output displacement and stress, next to is variable C, variable B and final is variable D. The data of Table 10 were also used to plot the graph, as shown in Figure 6. This figure also shows that variable A significantly affected on output displacement and stress. next to is variable C, variable B and final is variable D. As the slope of the graph increases, the influence increases.

The results of analysis of signal-to-noise ratios for GRG, B_i, and APS_i are exactly the same as the results of the grey relational analysis, TOPSIS method, MOORA method and finite element analysis.

4.8 Results of analysis of variance

The results of analysis of variance for GRG are presented in Table 11, which shows that the designed variables significantly affected the output displacement and stress. Because the F-values were all greater than 2, the P-values were all less than 0.05. Variable A have significantly affected the output displacement and stress, next to is variable C, variable B and final is variable D. The contribution percentages of A, C, B and D were 39.49%, 27.49%, 11.20% and 3.49%, respectively.

The values of S, R-square, R-square (adj), press and R-square (pred) were found to be 0.0684776, 98.35%, 96.86%, 0.569735 and 94.00%, respectively, as shown in Table 12. In Table 13, the value of R-square is over 98%. The problem that the reliability of the grey relational analysis method is very high.

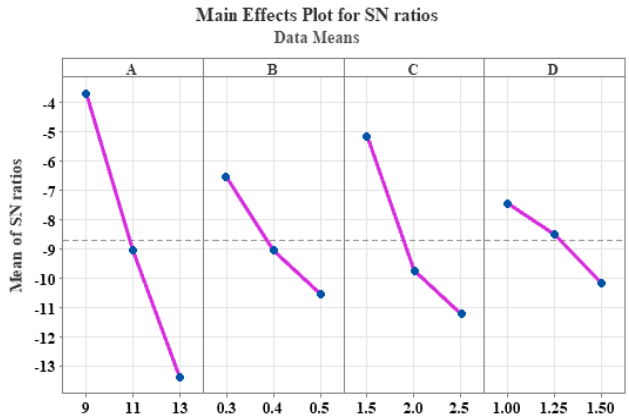

Figure 6. The graph analysis of signal-to-noise ratios for APS_i

Table 11. Results of the analysis of variance for GRG

Source	DF	Seq SS	Contribution	Adj SS	Seq MS	F-Value	P-Value
A	2	0.104351	39.49%	0.104351	0.052176	111.32	0.010
B	2	0.029605	11.20%	0.029605	0.014802	31.61	0.011
C	2	0.072643	27.49%	0.072643	0.036322	77.52	0.022
D	2	0.003932	3.49%	0.003932	0.001966	4.21	0.045
A*B	4	0.009490	5.59%	0.009490	0.002373	5.13	0.035
A*C	4	0.010382	5.93%	0.010382	0.002595	5.52	0.025
A*D	4	0.005696	5.16%	0.005696	0.001424	3.01	0.040
Error	6	0.028135	1.65%	0.028135	0.004689		
Total	26	0.264235	100.00%				

Table 12. Model summary for GRG

S	R-sq	R-sq(adj)	PRESS	R-sq(pred)
0.0684776	98.35%	96.86%	0.569735	94.00%

Table 13. Results analysis of variance for B_i

Source	DF	Seq SS	Contribution	Adj SS	Seq MS	F-Value	P-Value
A	2	0.183490	38.84%	0.183490	0.091745	87.39	0.000
B	2	0.043441	9.43%	0.043441	0.021721	20.69	0.002
C	2	0.163161	35.43%	0.163161	0.081581	77.71	0.000
D	2	0.022861	4.96%	0.022861	0.011431	10.89	0.010
A*B	4	0.022964	4.99%	0.022964	0.005741	8.47	0.033
A*C	4	0.012442	2.70%	0.012442	0.003110	4.96	0.041
A*D	4	0.005856	2.27%	0.005856	0.001464	3.90	0.045
Error	6	0.006299	1.38%	0.006299	0.001050		
Total	26	0.460515	100.00%				

Table 14. Model summary for B_i

S	R-sq	R-sq(adj)	PRESS	R-sq(pred)
0.0324014	98.62%	96.07%	0.127557	94.30%

The results of analysis of variance for B_i of TOPSIS method are presented in Table 13. It also shows that the designed variables significantly affected output displacement and stress. Because the F-values were all greater than 2, the P-values were all less than 0.05. The variable A significantly affected output displacement and stress, next to is variable C, variable B and final is variable D. The percentages of A, C, B and D were 38.84%, 35.43%, 9.43% and 4.96%, respectively.

The values S, R-square, R-square (adj), press and R-square (pred) were found to be 0.0684776, 98.35%, 96.86%, 0.569735 and 94.00%, respectively, as shown in Table 14. In Table 14, the value of R-square is also over 98%. The problem that the reliability of the TOPSIS method is very high.

The results of analysis of variance for B_i of TOPSIS method are presented in Table 15. Table 15 also shows that the designed variables significantly affected the output displacement and stress. Because the F-values were all greater than 2, the P-values were all less than 0.05. Variable A significantly affected on output displacement and stress, next to is variable C, variable B and final is variable D. Because the contribution percentage of A, C, B and D are 47.42%, 20.07%, 14.02% and 5.91%, respectively.

Table 15. Results analysis of variance for APS_i

Source	DF	Seq SS	Contribution	Adj SS	Seq MS	F-Value	P-Value
A	2	0.73965	47.42%	0.73965	0.369825	49.79	0.000
B	2	0.21865	14.02%	0.21865	0.109325	14.72	0.005
C	2	0.31300	20.07%	0.31300	0.156500	21.07	0.002
D	2	0.07659	5.91%	0.07659	0.038296	5.16	0.018
A*B	4	0.08706	5.58%	0.08706	0.021765	2.93	0.026
A*C	4	0.04545	2.91%	0.04545	0.011363	2.53	0.031
A*D	4	0.03466	2.22%	0.03466	0.008666	2.17	0.041
Error	6	0.04457	1.86%	0.04457	0.007428		
Total	26	1.55964	100.00%				

The values S, R-square, R-square (adj), press and R-square (pred) were found to be 0.0684776, 98.35%, 96.86%, 0.569735 and 94.00%, respectively, as shown in Table 16. Table 16 also shows that the value of R-square was over 98%.

Table 16. Model summary for APS_i

S	R-sq	R-sq(adj)	PRESS	R-sq(pred)
0.0861854	98.87%	97.02%	0.902492	95.13%

The results of the analysis of variance for GRG, B_i and APS_i were exactly the same as the grey relational analysis results, TOPSIS method results, MOORA method results, analysis of signal-to-noise ratios and finite element analysis results.

4.9 Results analysis of 3D surface plot

The graphs of the 3D surface for GRG are shown in Figure 7 In Figure 7(a), when variable A increased from 9 mm to 13 mm, the GRG values were reduced, whereas when variable B increased from 0.3 mm to 0.5 mm, the GRG values were reduced. This problem indicates that when thickness of flexure hinges increases, displacement decreases. The same is shown for variable C and variable D, as shown in Figure 7(b), when radius of the flexure hinges increases, the displacement decreases.

The graphs of 3D surface for B_i are shown in Figure 8. In Figure 8(a), when variable A increased from 9 mm to 13 mm, the B_i values were reduced, whereas when variable B increased from 0.3 mm to 0.5 mm, the GRG values were reduced. This problem indicates that when thickness of flexure hinges increases, the displacement decreases. The same is shown for variable C and variable D; as shown in Figure 8(b), when the radius of the flexure hinges increases, the displacement decreases.

The graphs of 3D surface for APS_i are shown in Figure 9. In Figure 9(a), when variable A increased from 9 mm to 13 mm, the APS_i values decreased, whereas when variable B increased from 0.3 mm to 0.5 mm, the GRG values decreased. This problem indicates that when thickness of flexure hinges increases, the displacement decreases. The same is shown for variable C and variable D; as indicated in Figure 9(b), when the radius of the flexure hinges increases, the displacement decreases.

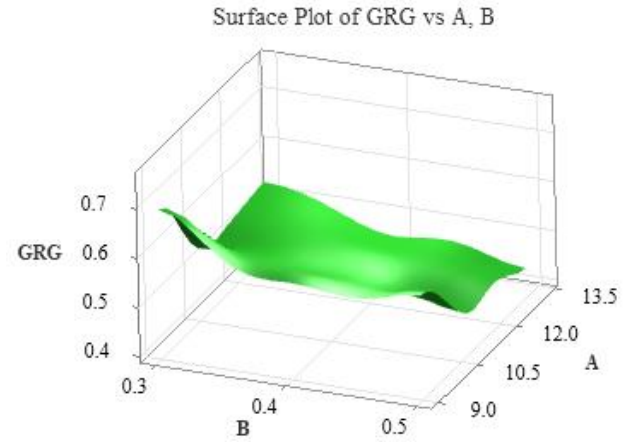

(a) Effect of variables A and B

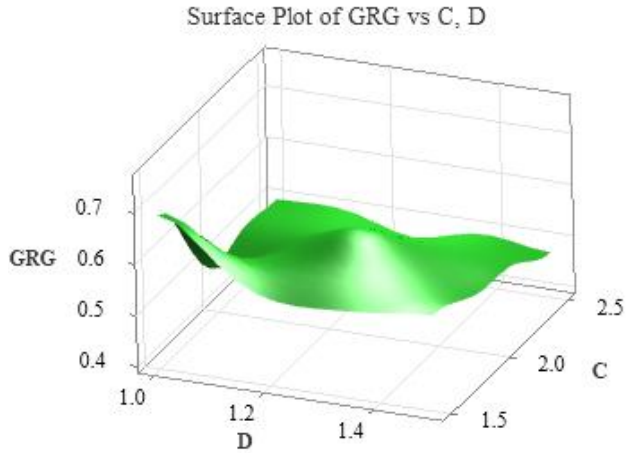

(b) Effect of variables C and D

Figure 7. Effect of the design variables on GRG

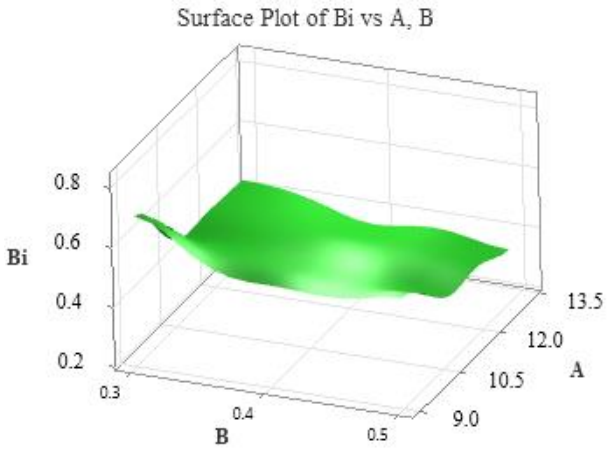

(a) Effect of variables A and B

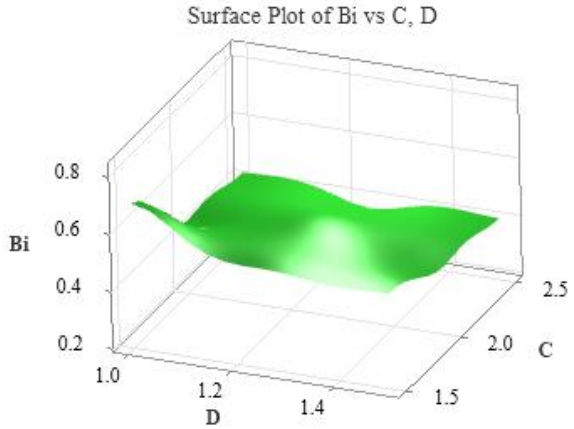

(b) Effect of variables C and D

Figure 8. Effect of the design variables on B_i

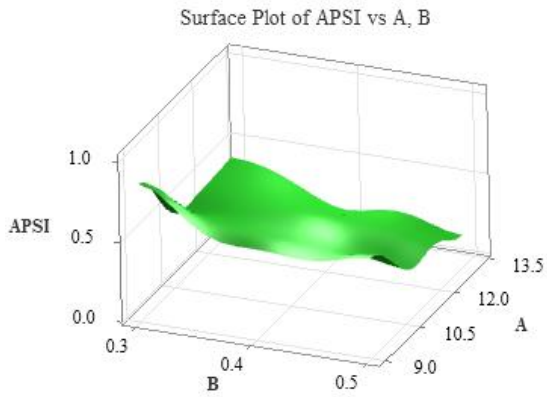

(a) Effect of the design variables A and B

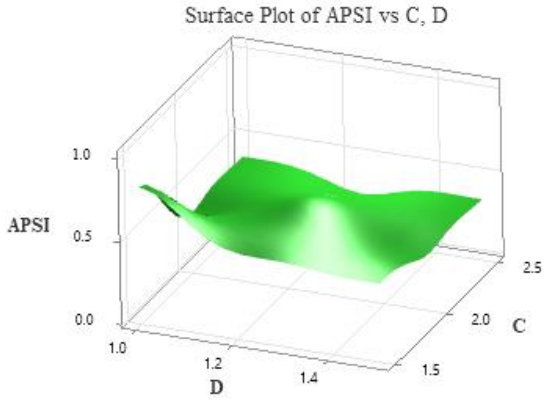

(b) Effect of the design variables C and D

Figure 9. Effect of the design variables on APS_i

The results of 3D surface plot for GRG, B_i and APS_i were exactly the same as the grey relational analysis results, TOPSIS method results, MOORA method results, signal-to-noise ratio analysis results and finite element results.

4.10 Confirmed results

The predicted values of GRG, B_i, Q_i, APS_i were 0.75415, 0.79362, 0.033199 and 1.10305, respectively. At an interval confidence of 95%, the CI values for GRG, B_i and ASP_i were found to be ±0.186, ±0.089, ±0.2367, respectively, by Eq. (37) for the following four optimization methods:

For GRG:

$$CI_{CE} = \pm\sqrt{5.9874 \times 0.004689 \times \left(\frac{1}{\frac{27}{1+6}}+1\right)} = \pm 0.186$$

$$0.553474 < \mu_{confirmation} < 0.92953$$

where, α = 0.05, fe = 6, $F_{0.05}(1,6)$ = 5.9874, Ve = 0.004689 [67], R = 6, Re = 1, n = 27.

For B_i:

$$CI_{CE} = \pm\sqrt{5.9874 \times 0.00105 \times \left(\frac{1}{\frac{27}{1+6}}+1\right)} = \pm 0.089$$

$$0.704644 < \mu_{confirmation} < 0.882596$$

where, α = 0.05, fe = 6, $F_{0.05}(1,19)$ = 5.9874, Ve = 0.00105 [67], R = 6, Re = 1, n = 27.

For APS_i:

$$CI_{CE} = \pm\sqrt{5.9874 \times 0.007428 \times \left(\frac{1}{\frac{27}{1+6}}+1\right)} = \pm 0.2367$$

$$0.866397 < \mu_{confirmation} < 1.339703$$

where, α = 0.05, Ve = 0.007428 [67], fe = 6, $F_{0.05}(1,19)$ = 5.9874, R = 6, Re = 1, n = 27.

In the first case, the optimal displacement and stress was found to be 0.11179 mm and 87.113 MPa through finite element analysis, while the input displacement was 0.01 mm. Therefore, the displacement amplification ratio was found to be over 11 times.

Table 17. Comparison of the predicted and optimal values

Factor	Predicted	Optimal	Error (%)
GRG	0.75415	0.7612	0.9262
B_i	0.79362	0.8196	3.1692
Q_i	0.036799	0.03440	6.5311
APS_i	1.10305	1.000	1.0199
Displacement (mm)	0.11276	0.1179	4.3596
Stress (MPa)	80.242	84.113	5.2307

As shown in Table 17, the predicted and optimal values of GRG, B_i, Q_i, APS_i were 0.75415 and 0.7542, 0.79362 and 0.8196, 0.033199 and 0.03112, and 1.10305 and 1.000, respectively. In Table 17, the predicted value of displacement and stress are shown to be 0.11276 mm and 80.242 MPa, while the optimal value of displacement and stress are 0.1179 and

84.113 MPa as presented in Figure 10. Thus, the error of the predicted and optimal values of GRG, B_i, Q_i, APS_i were 0.0012%, 3.1692%, 6.5311% and 1.01996%. Error values are less than 6%. Thus, this problem identified that the four methods used here are good agree and were also confirmed by analysis of signal-to-noise ratios, analysis of variance and analysis of the 3D graph surface plots. The optimal values of displacement and stress were 4.3596% and 5.2307%, respectively and the displacement amplification ratio was found to be over 11 times. These results are larger than the results previously found in reference [30].

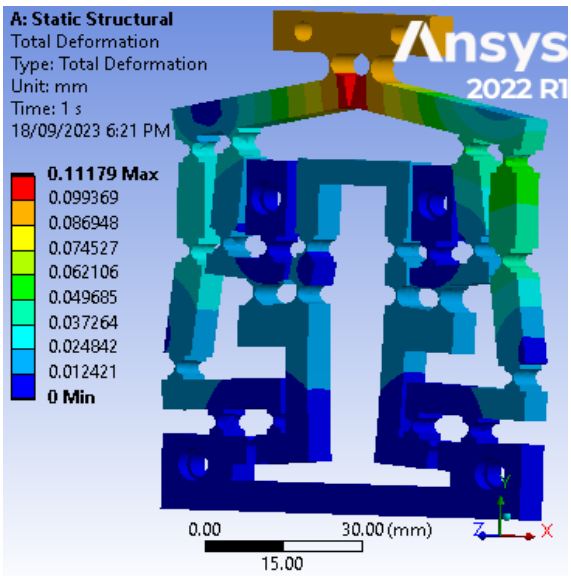

(a)Displacement

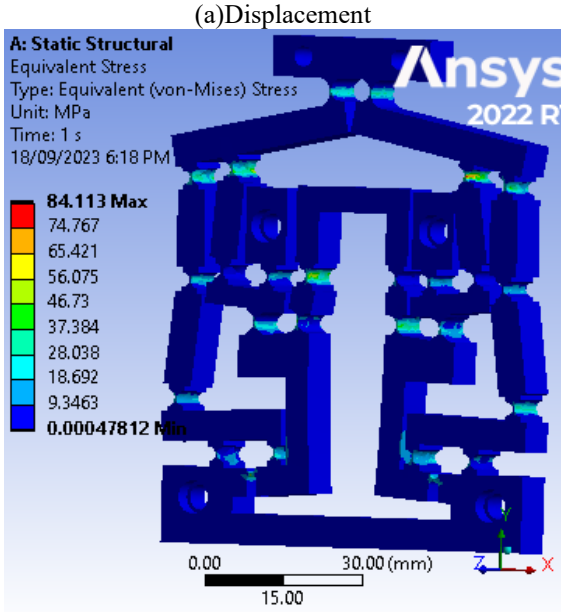

(b) Stress

Figure 10. The optimal result of displacement and equivalent (von-Mies) stress

5. CONCLUSIONS

In this investigation, we designed 27 models of a novel symmetrical differential lever displacement magnification compliant mechanism with SolidWorks. The design variables and their levels were selected as follows: Variable A consisted of three levels of 9 mm, 11 mm and 13 mm; variable B consisted of three levels of 0.3 mm, 0.4 mm and 0.5 mm; variable C consisted of three levels of 1.5 mm, 2 mm and 2.5 mm; variable D consisted of three levels of 1.0 mm, 1.25 mm and 1.5 mm. Twenty-seven cases for simulation were designed using Minitab experimental design software. Displacement and stress were analysed using finite element analysis in ANSYS. The results of FEM indicated that the design variables significantly affected the displacement and stress of the study model. The problem was verified by the results of analysis of signal-to-noise ratios of GRG, B_i, Q_i and APS_i. Additionally, the problem was also confirmed through analysis of variance and analysis of graphs of the 3D surface for GRG, B_i, Q_i and APS_i. Four optimization methods were selected, with the first case being the optimal case. The error of the four methods is less than 7%, and the optimal results for the displacement and stress were found to be 0.1179 mm and 84.113 MPa, respectively. The predicted values of the displacement and stress were found to be 0.11276 mm and 80.2421 MPa, respectively, with the input displacement equal to 0.01. Thus, the displacement amplification ratio obtained over 11 times. The limitation of this study is that the model has not been tested for displacement and stress amplification. Different types of flexure hinges have not been applied for comparison. Algorithms have not been developed to determine the displacement and stress amplification of the proposed model. Because these are costly and time-consuming. Therefore, these can be done in the future. In addition, the application of other optimization methods also contributes to increasing the reliability of the research results, such as Adaptive neuro fuzzy inference system, artificial neural network, SAW method, WASSPAS method decision making methods.

ACKNOWLEDGMENT

This work was financially supported by Ho Chi Minh City University of Industry and Trade under Contract No.: 75/HĐ-DCT dated 15th Aug. 2023.

REFERENCES

[1] Cao, L., Dolovich, A.T., Chen, A., Zhang, W.C. (2018). Topology optimization of efficient and strong hybrid compliant mechanisms using a mixed mesh of beams and flexure hinges with strength control. Mechanism and Machine Theory, 121: 213-227. https://doi.org/10.1016/j.mechmachtheory.2017.10.022

[2] Chen, F., Du, Z.J., Yang, M., Gao, F., Dong, W., Zhang, D. (2018). Design and analysis of a three-dimensional bridge-type mechanism based on the stiffness distribution. Precision Engineering, 51: 48-58. https://doi.org/10.1016/j.precisioneng.2017.07.010

[3] Chen, S., Ling, M., Zhang, X. (2018). Design and experiment of a millimeter-range and high-frequency compliant mechanism with two output ports. Mechanism and Machine Theory, 126: 201-209. https://doi.org/10.1016/j.mechmachtheory.2018.04.003

[4] Dong, W., Chen, F., Gao, F., Yang, M., Sun, L., Du, Z., Zhang, D. (2018). Development and analysis of a bridge-lever-type displacement amplifier based on hybrid flexure hinges. Precision Engineering, 54: 171-181. https://doi.org/10.1016/j.precisioneng.2018.04.017

[5] Choi, K.B., Lee, J.J., Kim, G.H., Lim, H.J., Kwon, S.G. (2018). Amplification ratio analysis of a bridge-type

mechanical amplification mechanism based on a fully compliant model. Mechanism and Machine Theory, 121: 355-372. https://doi.org/10.1016/j.mechmachtheory.2017.11.002

[6] Clark, L., Shirinzadeh, B., Pinskier, J., Tian, Y., Zhang, D. (2018). Topology optimisation of bridge input structures with maximal amplification for design of flexure mechanisms. Mechanism and Machine Theory, 122: 113-131. https://doi.org/10.1016/j.mechmachtheory.2017.12.017

[7] Chen, F., Cai, J., Dong, W., Du, Z. (2019). A generalized mathematical model for the bridge-type and lever-type mechanism. In Intelligent Robotics and Applications: 12th International Conference, ICIRA 2019, Shenyang, China, pp. 296-309. https://doi.org/10.1007/978-3-030-27526-6_26

[8] He, Y., Zou, P., Zhu, Z., Zhu, W.L., Yang, X., Cao, J., Ehmann, K.F. (2018). Design and application of a flexure-based oscillation mechanism for surface texturing. Journal of Manufacturing Processes, 32: 298-306. https://doi.org/10.1016/j.jmapro.2018.02.017

[9] Herpe, X., Walker, R., Dunnigan, M., Kong, X. (2018). On a simplified nonlinear analytical model for the characterisation and design optimisation of a compliant XY micro-motion stage. Robotics and Computer-Integrated Manufacturing, 49: 66-76. https://doi.org/10.1016/j.rcim.2017.05.012

[10] Liang, C., Wang, F., Shi, B., Huo, Z., Zhou, K., Tian, Y., Zhang, D. (2018). Design and control of a novel asymmetrical piezoelectric actuated microgripper for micromanipulation. Sensors and Actuators A: Physical, 269: 227-237. https://doi.org/10.1016/j.sna.2017.11.027

[11] Lin, C., Shen, Z., Wu, Z., Yu, J. (2018). Kinematic characteristic analysis of a micro-/nano positioning stage based on bridge-type amplifier. Sensors and Actuators A: Physical, 271: 230-242. https://doi.org/10.1016/j.sna.2017.12.030

[12] Ling, M., Cao, J., Howell, L.L., Zeng, M. (2018). Kinetostatic modeling of complex compliant mechanisms with serial-parallel substructures: A semi-analytical matrix displacement method. Mechanism and Machine Theory, 125: 169-184. https://doi.org/10.1016/j.mechmachtheory.2018.03.014

[13] Ling, M., Cao, J., Jiang, Z., Lin, J. (2018). A semi-analytical modeling method for the static and dynamic analysis of complex compliant mechanism. Precision Engineering, 52: 64-72. https://doi.org/10.1016/j.precisioneng.2017.11.008

[14] Ling, M., Chen, S., Li, Q., Tian, G. (2018). Dynamic stiffness matrix for free vibration analysis of flexure hinges based on non-uniform Timoshenko beam. Journal of Sound and Vibration, 437: 40-52. https://doi.org/10.1016/j.jsv.2018.09.013

[15] Linß, S., Gräser, P., Räder, T., Henning, S., Theska, R., Zentner, L. (2018). Influence of geometric scaling on the elasto-kinematic properties of flexure hinges and compliant mechanisms. Mechanism and Machine Theory, 125: 220-239. https://doi.org/10.1016/j.mechmachtheory.2018.03.008

[16] Šalinić, S., Nikolić, A. (2018). A new pseudo-rigid-body model approach for modeling the quasi-static response of planar flexure-hinge mechanisms. Mechanism and Machine Theory, 124: 150-161. https://doi.org/10.1016/j.mechmachtheory.2018.02.011

[17] Wu, Z., Xu, Q. (2018). Design, optimization and testing of a compact XY parallel nanopositioning stage with stacked structure. Mechanism and Machine Theory, 126: 171-188. https://doi.org/10.1016/j.mechmachtheory.2018.04.008

[18] Zhu, W. L., Zhu, Z., Guo, P., Ju, B.F. (2018). A novel hybrid actuation mechanism based XY nanopositioning stage with totally decoupled kinematics. Mechanical Systems and Signal Processing, 99: 747-759. https://doi.org/10.1016/j.ymssp.2017.07.010

[19] Zhu, Z., To, S., Li, Y., Zhu, W.L., Bian, L. (2018). External force estimation of a piezo-actuated compliant mechanism based on a fractional order hysteresis model. Mechanical Systems and Signal Processing, 110: 296-306. https://doi.org/10.1016/j.ymssp.2018.03.012

[20] Ling, M. (2019). A general two-port dynamic stiffness model and static/dynamic comparison for three bridge-type flexure displacement amplifiers. Mechanical Systems and Signal Processing, 119: 486-500. https://doi.org/10.1016/j.ymssp.2018.10.007

[21] Ling, M., Cao, J., Pehrson, N. (2019). Kinetostatic and dynamic analyses of planar compliant mechanisms via a two-port dynamic stiffness model. Precision Engineering, 57: 149-161. https://doi.org/10.1016/j.precisioneng.2019.04.004

[22] Wang, F., Shi, B., Tian, Y., Huo, Z., Zhao, X., Zhang, D. (2019). Design of a novel dual-axis micromanipulator with an asymmetric compliant structure. IEEE/ASME Transactions on Mechatronics, 24(2): 656-665. https://doi.org/10.1109/tmech.2019.2893681

[23] Wang, J., Li, J., Xu, Z., Wang, S., Wang, Z., Xu, B., Zhao, H. (2019). Design, analysis, experiments and kinetic model of a high step efficiency piezoelectric actuator. Mechatronics, 59: 61-68. https://doi.org/10.1016/j.mechatronics.2019.03.003

[24] Das, T.K., Shirinzadeh, B., Ghafarian, M., Al-Jodah, A., Pinskier, J. (2020). Characterization of a compact piezoelectric actuated microgripper based on double-stair bridge-type mechanism. Journal of Micro-Bio Robotics, 16: 79-92. https://doi.org/10.1007/s12213-020-00132-5

[25] Lin, C., Zheng, S., Li, P., Jiang, M. (2021). Kinetostatic analysis of 6-DOF compliant platform with a multi-stage condensed modeling method. Microsystem Technologies, 27: 2153-2166. https://doi.org/10.1007/s00542-020-05029-8

[26] Zhang, Q., Zhao, J., Peng, Y., Pu, H., Yang, Y. (2020). A novel amplification ratio model of a decoupled XY precision positioning stage combined with elastic beam theory and Castigliano's second theorem considering the exact loading force. Mechanical Systems and Signal Processing, 136: 106473. https://doi.org/10.1016/j.ymssp.2019.106473

[27] Lin, C., Jiang, M., Zheng, S. (2021). Establishment and verification of the analytical model for the critical parameters in the kinematics model of the precision positioning stage. Sensors and Actuators A: Physical, 320: 112572. https://doi.org/10.1016/j.sna.2021.112572

[28] Fan, W., Jin, H., Fu, Y., Lin, Y. (2021). A type of symmetrical differential lever displacement amplification mechanism. Mechanics & Industry, 22: 5. https://doi.org/10.1051/meca/2021003

[29] Zhang, W., Yan, P. (2024). A variable stiffness compliant actuator based on antagonistic normal-stressed

electromagnetic mechanism. Sensors and Actuators A: Physical, 366: 114983. https://doi.org/10.1016/j.sna.2023.114983
[30] Wu, H., Tang, H., Qin, Y. (2024). Design and test of a 2-DOF compliant positioning stage with antagonistic piezoelectric actuation. Machines, 12(6): 420. https://doi.org/10.3390/machines12060420
[31] Wang, Y., Zhang, L., Meng, L., Lu, H., Ma, Y. (2024). Theoretical modeling and experimental verification of elliptical hyperbolic hybrid flexure hinges. Symmetry, 16(3): 345. https://doi.org/10.3390/sym16030345
[32] Wei, H., Tian, Y., Zhao, Y., Ling, M., Shirinzadeh, B. (2023). Two-axis flexure hinges with variable elliptical transverse cross-sections. Mechanism and Machine Theory, 181: 105183. https://doi.org/10.1016/j.mechmachtheory.2022.105183
[33] Meng, Q., Chen, Z., Kang, H., Shen, Z., Yu, H. (2023). Analytical modeling and application for semi-circular notch flexure hinges. Applied Sciences, 13(16): 9248. https://doi.org/10.3390/app13169248
[34] Keshavarz-Ghorabaee, M., Amiri, M., Zavadskas, E.K., Turskis, Z., Antucheviciene, J. (2021). Determination of objective weights using a new method based on the removal effects of criteria (MEREC). Symmetry, 13(4): 525. https://doi.org/10.3390/sym13040525
[35] Keshavarz-Ghorabaee, M. (2021). Assessment of distribution center locations using a multi-expert subjective–objective decision-making approach. Scientific Reports, 11(1): 19461. https://doi.org/10.1038/s41598-021-98698-y
[36] Banik, B., Alam, S., Chakraborty, A. (2023). Comparative study between GRA and MEREC technique on an agricultural-based MCGDM problem in pentagonal neutrosophic environment. International Journal of Environmental Science and Technology, 20: 1-16. https://doi.org/10.1007/s13762-023-04768-1
[37] Mishra, A.R., Saha, A., Rani, P., Hezam, I.M., Shrivastava, R., Smarandache, F. (2022). An integrated decision support framework using single-valued-MEREC-MULTIMOORA for low carbon tourism strategy assessment. IEEE Access, 10: 24411-24432. https://doi.org/10.1109/access.2022.3155171
[38] Ecer, F., Aycin, E. (2022). Novel comprehensive MEREC weighting-based score aggregation model for measuring innovation performance: The case of G7 countries. Informatica, 34(1): 53-83. https://doi.org/10.15388/22-infor494
[39] Hezam, I.M., Mishra, A.R., Rani, P., Cavallaro, F., Saha, A., Ali, J., Strielkowski, W., Štreimikienė, D. (2022). A hybrid intuitionistic fuzzy-MEREC-RS-DNMA method for assessing the alternative fuel vehicles with sustainability perspectives. Sustainability, 14(9): 5463. https://doi.org/10.3390/su14095463
[40] Shanmugasundar, G., Sapkota, G., Čep, R., Kalita, K. (2022). Application of MEREC in multi-criteria selection of optimal spray-painting robot. Processes, 10(6): 1172. https://doi.org/10.3390/pr10061172
[41] Silva, N.F., dos Santos, M., Gomes, C.F.S., de Andrade, L.P. (2023). An integrated CRITIC and Grey Relational Analysis approach for investment portfolio selection. Decision Analytics Journal, 8: 100285. https://doi.org/10.1016/j.dajour.2023.100285
[42] Meel, R., Singh, V., Katyal, P., Gupta, M. (2022). Optimization of process parameters of micro-EDD/EDM for magnesium alloy using Taguchi based GRA and TOPSIS method, Materials Today: Proceedings, 51: 269-275. https://doi.org/10.1016/j.matpr.2021.05.287
[43] Chanakyan, C., Sivasankar, S., Meignanamoorthy, M., Alagarsamy, S.V. (2021). Parametric optimization of mechanical properties via FSW on AA5052 using Taguchi based grey relational analysis. Incas Bulletin, 13(2): 21-30. https://doi.org/10.13111/2066-8201.2021.13.2.3
[44] Abifarin, J.K. (2021). Taguchi grey relational analysis on the mechanical properties of natural hydroxyapatite: Effect of sintering parameters. The International Journal of Advanced Manufacturing Technology, 117: 49-57. https://doi.org/10.1007/s00170-021-07288-9
[45] Ikeagwuani, C.C., Agunwamba, J.C., Nwankwo, C.M., Eneh, M. (2020). Additives optimization for expansive soil subgrade modification based on Taguchi grey relational analysis. International Journal of Pavement Research and Technology, 14: 138-152. https://doi.org/10.1007/s42947-020-1119-4
[46] Awale, A., Inamdar, K. (2020). Multi-objective optimization of high-speed turning parameters for hardened AISI S7 tool steel using grey relational analysis. Journal of the Brazilian Society of Mechanical Sciences and Engineering, 42: 356. https://doi.org/10.1007/s40430-020-02433-z
[47] Sarıkaya, M., Güllü, A. (2015). Multi-response optimization of minimum quantity lubrication parameters using Taguchi-based grey relational analysis in turning of difficult-to-cut alloy Haynes 25. Journal of Cleaner Production, 91: 347-357. https://doi.org/10.1016/j.jclepro.2014.12.020
[48] Sheth, M., Gajjar, K., Jain, A., Shah, V., Patel, H., Chaudhari, R., Vora, J. (2021). Multi-objective Optimization of Inconel 718 Using Combined Approach of Taguchi—Grey Relational Analysis. In Advances in Mechanical Engineering, pp. 229-235, Springer, Singapore. https://doi.org/10.1007/978-981-15-3639-7_27
[49] Niranjan, T., Singaravel, B., Raju, S.S. (2022). Optimization of hole quality parameters using TOPSIS method in drilling of GFRP composite. Materials Today: Proceedings, 62: 2109-2114. https://doi.org/10.1016/j.matpr.2022.03.042
[50] Prabhuram, T., Singh, S.P., Durairaj, J.I., Elilraja, D., Das, M.C., Sunderraj, D.A.J. (2022). Optimization of operation parameters in machining of functionally graded metal matrix composite using TOPSIS. Materials Today: Proceedings, 62: 429-433. https://doi.org/10.1016/j.matpr.2022.03.562
[51] Singh, G., Kumar, A., Aggarwal, V., Singh, S. (2022). Experimental investigations and optimization of machining performance during turning of EN-31 steel using TOPSIS approach. Materials Today: Proceedings, 48: 1089-1094. https://doi.org/10.1016/j.matpr.2021.07.381
[52] Kanagaraju, T., Gowthaman, B., Arunkumar, A., Akash, S. (2022). Optimization of machining parameters in wet and cryogenic machining using TOPSIS approach. Materials Today: Proceedings, 62: 1157-1162. https://doi.org/10.1016/j.matpr.2022.04.346
[53] Chakraborty, S., Chatterjee, P. (2017). A developed meta-model for selection of cotton fabrics using design of experiments and TOPSIS method. Journal of the

Institution of Engineers (India): Series E, 98: 79-90. https://doi.org/10.1007/s40034-017-0108-x
[54] Brauers, W.K. (2013). Optimization Methods for a Stakeholder Society: A Revolution in Economic Thinking by Multi-Objective Optimization. Springer Science & Business Media.
[55] Gorener, A., Dinçer, H., Hacioglu, U. (2013). Application of multi-objective optimization on the basis of ratio analysis (MOORA) method for bank branch location selection. International Journal of Finance & Banking Studies, 2(2): 41-52. https://doi.org/10.20525/ijfbs.v2i2.145
[56] Mitra, A. (2022). Application of multi-objective optimization on the basis of ratio analysis (MOORA) for selection of cotton fabrics for optimal thermal comfort. Research Journal of Textile and Apparel, 26(2): 187-203. https://doi.org/10.1108/rjta-02-2021-0021
[57] Chakraborty, S., Datta, H.N., Kalita, K., Chakraborty, S. (2023). A narrative review of multi-objective optimization on the basis of ratio analysis (MOORA) method in decision making. Opsearch, 60(4): 1844-1887. https://doi.org/10.1007/s12597-023-00676-7
[58] Wei, G., Wei, C., Guo, Y. (2021). EDAS method for probabilistic linguistic multiple attribute group decision making and their application to green supplier selection. Soft Computing, 25(14): 9045-9053. https://doi.org/10.1007/s00500-021-05842-x
[59] He, Y., Lei, F., Wei, G., Wang, R., Wu, J., Wei, C. (2019). EDAS method for multiple attribute group decision making with probabilistic uncertain linguistic information and its application to green supplier selection. International Journal of Computational Intelligence Systems, 12(2): 1361-1370. https://doi.org/10.2991/ijcis.d.191028.001
[60] Peng, D., Wang, J., Liu, D., Liu, Z. (2022). An improved EDAS method for the multi-attribute decision making based on the dynamic expectation level of decision makers. Symmetry, 14(5): 979. https://doi.org/10.3390/sym14050979
[61] Sharma, A., Belokar, R.M., Kumar, S. (2018). Multi-response optimization of Al2024/red mud MMC using hybrid Taguchi-GRA-entropy optimization technique. Materials Today: Proceedings, 5(2): 4748-4760. https://doi.org/10.1016/j.matpr.2017.12.048
[62] Prasad, K.S. Chaitanya, G. (2021). Optimization of process parameters on surface roughness during drilling of GFRP composites using Taguchi technique. Materials Today: Proceedings, 39: 1553-1558. https://doi.org/10.1016/j.matpr.2020.05.562
[63] Patel, N.S., Parihar, P.L., Makwana, J.S. (2021). Parametric optimization to improve the machining process by using Taguchi method: A review. Materials Today: Proceedings, 47: 2709-2714. https://doi.org/10.1016/j.matpr.2021.03.005
[64] Dutta, S., Narala, S.K.R. (2021). Optimizing turning parameters in the machining of AM alloy using Taguchi methodology. Measurement, 169: 108340. https://doi.org/10.1016/j.measurement.2020.108340
[65] Radhwan, H., Shayfull, Z., Nasir, S.M., el-hadj Abdellah, A., Irfan, A.R. (2020). Optimization parameter effects on the quality surface finish of 3D-printing process using Taguchi method. IOP Conference Series: Materials Science and Engineering, 864(1): 012143. https://doi.org/10.1088/1757-899x/864/1/012143
[66] Chen, W.C., Hsu, Y.Y., Hsieh, L.F., Tai, P.H. (2010). A systematic optimization approach for assembly sequence planning using Taguchi method, DOE, and BPNN. Expert Systems with Applications, 37(1): 716-726. https://doi.org/10.1016/j.eswa.2009.05.098
[67] Roy, R.K. (2010). A primer on the Taguchi method. Society of Manufacturing Engineers.